Macromolecules

ARTICLE

pubs.acs.org/Macromolecules

Impact of Monomer Sequence, Composition and Chemical Heterogeneity on Copolymer-Mediated Effective Interactions between Nanoparticles in Melts

Lisa M. Hall[†,§] and Kenneth S. Schweizer*[,†,‡]

[†]Department of Chemical and Biomolecular Engineering and [‡]Department of Materials Science and Engineering, University of Illinois at Urbana−Champaign, Urbana, Illinois 61801, United States

ABSTRACT: The microscopic polymer reference interaction site model theory is applied to study the structural correlations of dilute spherical nanoparticles dissolved in AB copolymer melts of variable architecture (alternating, random), composition, and monomer−nanoparticle adsorption strengths that span the depletion, steric stabilization, and bridging regimes. Comparison of the calculations of the monomer−particle pair correlations and polymer-mediated nanoparticle potential of mean force (PMF) with the behavior of reference homopolymers and a binary AB blend are also performed. All intermonomer potentials are hard core, which precludes polymer macrophase or microphase separation, thereby allowing the consequences of differential monomer wettability on nanoparticle spatial organization to be isolated. For each copolymer case, one monomer species adsorbs more strongly on the filler than the other, mimicking a specific attraction. The PMF for the alternating copolymer is similar to that of an analogous homopolymer with additional spatial modulation or layering features. Random copolymers, and the polymer blend, mediate a novel strong and spatially long-range attractive bridging type interaction between nanoparticles at moderate to high adsorption strengths. The depth of this attraction in the PMF is a nonmonotonic function of random copolymer composition, reflecting subtle competing enthalpic and entropic considerations. Virial-based estimates of the maximum solubility of nanoparticles are computed.

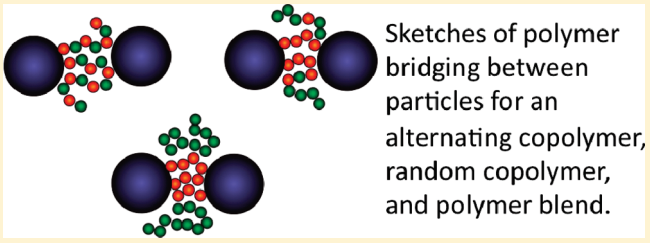

I. INTRODUCTION

The addition of nanoparticles to polymer melts or solids to create polymer nanocomposites (PNCs) is a powerful way to modify material properties. To maximize the effect of the nanoparticles on the polymer matrix, good spatial dispersion is often desired but is difficult to achieve in many real materials.[1−3] In certain applications, aggregates of controlled size, or even a percolating particle network, may instead be desired. The spatial organization of nanoparticles in a polymer matrix is ultimately determined by direct and polymer-mediated interactions. Thus, a key question in the design of PNCs is how to understand and design these effective interparticle interactions as a function of tunable chemical and physical variables.

Much recent experimental, theoretical, and simulation work has focused on spherical nanoparticles in a homopolymer melt and how to uniformly disperse them. If specific long-range spatial ordering and/or controlled spatial heterogeneity of nanoparticles is desired, microphase-separating block copolymers can be employed where the differential solubility in distinct microdomains can be utilized as a patterning tool.[4] Recently, nanoparticles have been added to copolymers with triblock, star, or alternating-block architectures.[5,6] However, few studies have investigated non-microphase-separating copolymers (e.g., random or alternating copolymers),[7−10] which is the focus of the present theoretical study. Such AB copolymers provide a much larger parameter space than can be realized for homopolymers because of the ability to rationally manipulate copolymer architecture (sequence) and composition and the difference in interaction of the A and B monomers with nanoparticles. Tuning such variables could help achieve more precise control of polymer-mediated interparticle interactions and nanoparticle dispersion.

Recent experiments have demonstrated the potential of using random copolymers to improve spatially homogeneous nanofiller dispersion. Specifically, a copolymer of styrene and vinylphenol of an intermediate composition improves the dispersion of functionalized carbon nanotubes (CNTs) relative to that in either the polystyrene or poly(vinylphenol) homopolymer.[7,8,10] The CNTs were functionalized such that they can hydrogen-bond with the phenolic monomer. Electron donor−acceptor interactions with unfunctionalized CNTs were also studied.[9] In this group of studies, monomers that interact very favorably (specific attractions much stronger than thermal energy) with CNTs were randomly copolymerized at various compositions with almost chemically identical monomers that do not strongly interact (far weaker nonspecific attraction) with the nanotubes. If the corresponding A and B monomers are homopolymers and blended, the mixture would be characterized by a small Flory χ-

Received: January 13, 2011
Revised: February 25, 2011
Published: March 17, 2011

parameter. The optimum copolymer composition for CNT dispersion was found to be an intermediate one for each of the three types of random copolymers studied. We note that the absolute level of CNT miscibility is still low, and the issue of whether the dispersion is truly equilibrated, versus kinetically trapped, is unsettled. A strong specific monomer−filler attraction with only one copolymer monomer is the key feature, and theoretically understanding the basic consequences of this type of interaction is the primary goal of the present work. Although our present focus is not carbon nanotubes, the physics underlying using random copolymers to improve dispersion of related systems such as spherical C_{60} buckyballs is expected to be quite similar, and our work is relevant to future experimental studies of such nanocomposites.

The polymer reference interaction site model (PRISM) theory[11] has previously been extensively applied to PNCs consisting of hard nanoparticles in a homopolymer melt.[11−18] Dilute spherical[12−15,17,18] and nonspherical[16] fillers have been studied. Predictions for nanospheres compare favorably with computer simulations in the one- and two-particle limits[12,17] and also with experimental scattering measurements on silica-based PNCs over a wide range of wavevectors and nondilute nanoparticle volume fractions under both melt and concentrated solution conditions.[19−21] Typically, the polymer−particle attraction strength is varied, and its effect on the polymer-mediated filler−filler potential of mean force (PMF) is the key quantity studied. For all high polymer concentration cases, local nanoscale packing effects play a crucial role in determining the PMF. For zero or very weak (compared to thermal energy, kT) monomer−particle attraction, entropic effects lead to a depletion attraction favoring particle contact and aggregation. At intermediate and high attraction strengths, the PMF is repulsive at short distances corresponding to an adsorbed polymer layer around each particle. At high polymer−particle attractions, enthalpy dominates, resulting in PMF minima at discrete nanoparticle surface separations corresponding to tight polymer bridging (sharing of the adsorbed layer) between nanoparticles and the formation of polymer−particle complexes. However, for intermediate attraction strength, there is a balance of entropic and enthalpic driving forces, and the adsorbed layers around each nanoparticle remain discrete, leading to a repulsive PMF (steric stabilization) and equilibrium nanoparticle dispersion and miscibility. The PMF in the two-particle limit is qualitatively similar to that found at higher particle volume fractions,[18] though many-body effects generally suppress miscibility[18] and mixture effective packing fraction changes with filler concentration are important for a quantitative understanding of experimental scattering patterns and statistical microstructure.[20] Less microscopic theories that do not take into account monomer scale packing effects have also been applied to study dispersion of nanoparticles in a homopolymer or block copolymer matrix, as recently reviewed.[22,23]

The consequences of replacing the homopolymer matrix with a nonmicrophase-separating copolymer or polymer blend on nanoparticle organization under dense melt conditions have not been explored with PRISM theory. Here, we extend this theory to address the chemical heterogeneity and sequence disorder effects characteristic of random copolymers. We consider the most basic case of hard nanospheres in AB copolymer melts and blends. Since our interest is to isolate and understand the role of differential attraction energies for the A and B monomers with the nanoparticle, the models studied are constructed so that polymer macrophase or microphase separation does not occur. Therefore, we vary A and B monomer−filler attraction strengths while holding all monomer−monomer interactions constant. This corresponds to a limiting hypothetical case where in the absence of nanoparticles the system is a homopolymer melt. Generalization beyond this model to treat the systems where the pure polymer matrix is not a homopolymer melt is straightforward within the PRISM framework.

The remainder of the paper is structured as follows. Section II discusses the models employed and PRISM theory for nanoparticles in copolymer melts. Section III presents calculations of the monomer−nanoparticle pair correlations in the dilute filler limit as a function of A and B interfacial attraction strengths and copolymer composition and architecture. Comparisons with the behavior of alternating copolymers, the A/B polymer blend, and reference homopolymers are also performed. Section IV presents the corresponding results for the copolymer-mediated PMF between nanoparticles, while spinodal demixing volume fractions are determined in the virial limit in section V. The paper concludes with a summary in section VI.

II. THEORY AND MODEL

To explore the effect of AB copolymer architecture on nanocomposite structure, spherical fillers in the dilute limit are studied in a random AB copolymer, an alternating AB copolymer, and a blend of A and B homopolymers. The calculations will be contrasted with the corresponding behavior in pure A or B homopolymer melts and with a hypothetical "average homopolymer" melt under identical chemical conditions. Most of the parameters and equations used have been described and motivated in prior homopolymer-based PRISM theory work.[13−15,18] However, several important differences arise upon consideration of a copolymer matrix. In the following equations, the subscript "p" denotes any polymer segment, "A" and "B" denote the two types of polymer segments, and "n" denotes a nanoparticle. The monomer diameter (same for A and B) is d and is the unit of length; energies are reported in units of the thermal energy, kT.

A. Three-Component PRISM Theory. PRISM theory for homopolymer liquids is an extension of the reference interaction site model (RISM) theory for small rigid molecules to polymers in which end effects are ignored or preaveraged (monomers are assumed to all have identical interchain correlation functions).[11] The theory has been extended and applied to phase-separating polymer mixtures,[11,24] diblock copolymers,[11,25] and regular multiblock[26] copolymers and, most recently, copolymers with variable level of sequence disorder[27] and fillers in homopolymer melts and concentrated solutions.[12−18,23] Each molecular species is composed of sites which intermolecularly interact in a pair decomposable manner. Given the site number densities and intramolecular correlations, the theory predicts the intermolecular site−site pair correlations, partial static structure factors, thermodynamic properties, and spinodal phase separation. For PNCs with a chemically heterogeneous polymer, chain end and AB junction effects on structural pair correlations are preaveraged (as done in prior copolymer PRISM studies[11]). Hence, for the AB copolymer there are two types of inequivalent monomer sites.

The statistical structure (averaged over thermal conformations and primary sequence if there is randomness) of monomers of

type i and j in a single chain is described by the real space intramolecular probability distribution function

$$\omega_{ij}(r) = \frac{1}{N_{\text{norm}}} \sum_{\alpha,\gamma=1}^{N} \omega_{\alpha\gamma}(r) \tag{1}$$

where $\omega_{\alpha\gamma}(r)$ is a normalized probability density of finding sites γ of type i and α of type j a distance r apart on the same molecule and N_{norm} is a normalization factor equal to N_i for $i = j$ and $N_i + N_j$ for $i \neq j$, where N_j is the mean number of j monomers in a polymer chain. For the nanosphere, $\omega_{nn}(k) = 1$. The AB copolymer is described by three intramolecular correlation functions: one for each type of site and a cross term. Any quenched chemical sequence disorder enters the theory in a preaveraged manner.[27] Expressions for the three site−site Fourier space $\omega(k)$ functions for an AB block copolymer with a variable probability of A−A and B−B block connectivity (versus A−B block connectivity) were derived for Markov chain models by Sung and Yethiraj.[27] In the present article, only the case of single monomer "blocks" is explored, though the "monomer correlation strength" λ is varied. The latter is given by $\lambda \equiv p_{AA} + p_{BB} - 1$, where p_{ij} is the probablility that a monomer of type i is followed by one of type j which depends on the polymer synthesis method.[27]

Three models are investigated: alternating copolymer ($\lambda = -1$), random copolymer ($\lambda = 0$), and polymer blend limit ($\lambda \rightarrow 1$). As motivated and used in prior work,[13,18,20] the polymer is modeled as a freely jointed chain consisting of $N_{\text{tot}} = 100$ segments with monomer site diameter d and bond (persistence) length $l = 4d/3$. The total polymer liquid packing fraction is fixed at a dense meltlike value of $\eta_t = 0.4$. The $\omega_{ij}(k)$ matrix in Fourier space for an ideal freely jointed chain with A and B monomers is given by[27]

$$\omega_{ii}(k) = \frac{1}{N_i} N_{\text{tot}} f_i + \frac{2}{N_i} \sum_{\tau=1}^{N_{\text{tot}}+1} (N_{\text{tot}} - \tau) (f_i^2 + f_i(1 - f_i)\lambda^\tau) \left(\frac{\sin(kl)}{kl}\right)^\tau \tag{2}$$

$$\omega_{AB}(k) = \frac{2}{N_{\text{tot}}} \sum_{\tau=1}^{N_{\text{tot}}+1} (N_{\text{tot}} - \tau) f_A f_B (1 - \lambda^\tau) \left(\frac{\sin(kl)}{kl}\right)^\tau \tag{3}$$

where N_{tot} is the total number of monomers in a chain and f_i is the fraction of i monomers; f_A is fixed at 0.5 for the alternating copolymer and polymer blend. Most random copolymer calculations are also performed at $f_A = 0.5$, with a few calculations presented over the full range $f_A = 0 \rightarrow 1$. We note that use of the ideal freely jointed chain model ignores conformational nonideality effects, which are expected to be of minor significance under the nearly incompressible meltlike conditions of interest. Moreover, in an ensemble-averaged sense, such effects are rigorously negligible in the infinitely dilute nanoparticle limit of present interest.

The matrix Ornstein−Zernike or Chandler−Andersen equations[28] relate the site−site intermolecular pair correlation functions, g, to the site−site intermolecular direct correlation functions C, via the coupled matrix integral equations in Fourier space:

$$\mathbf{H}(k) = \Omega(k)\mathbf{C}(k)[\Omega(k) + \mathbf{H}(k)] \tag{4}$$

Here, the $\mathbf{H}(k)$ and $\mathbf{C}(k)$ matrices have elements that are the Fourier transforms of $\rho_i\rho_j h_{ij}(r) = \rho_i\rho_j(g_{ij}(r) - 1)$ and $C_{ij}(r)$, respectively, and $\mathbf{\Omega}(k)$ is the intrachain structure factor matrix defined in terms of $\omega(k)$ weighted by the site densities with the normalizations chosen such that $\Omega_{ij}(k{=}0) = \rho_i N_j$. Using the normalization in eq1, the diagonal $\Omega_{ii} = \rho_i\omega_{ii}$ and the cross terms are $\Omega_{ij} = (\rho_i + \rho_j)\omega_{ij}$. Equation 4 with three types of sites (A, B, and nanoparticle) in general corresponds to six coupled nonlinear integral equations. For the specific copolymer model studied in this article the computational complexity is reduced because the integral equations can be solved sequentially in the dilute filler limit.[12,13]

Approximate closures that relate $h_{ij}(r)$, $C_{ij}(r)$, and the site−site potential functions, $U_{ij}(r)$, are required to have a solvable set of coupled equations. For phase-separating polymer blends and copolymers, so-called molecular closures are required to properly describe long wavelength concentration fluctuations and phase separation.[11,24] However, these are not necessary in our present work since in the absence of nanoparticles the polymer liquid is (by construction) a homopolymer melt and our focus is solely on the consequences of polymer−particle interactions. Hence, the classic "atomic closures" employed in previous homopolymer PNC−PRISM studies are reliable.[23] Prior PNC PRISM homopolymer predictions have been compared with molecular dynamics simulations in the dilute one- and two-particle limits,[12] and good agreement was found based on the site−site Percus−Yevick (PY) closure (eq 5) for polymer−polymer and polymer−nanoparticle interactions and the hypernetted chain closure (eq 6) for nanoparticle−nanoparticle interactions

$$C(r) = (e^{-U(r)} - 1)(1 + \gamma(r)) \tag{5}$$

$$C(r) = e^{\gamma(r) - U(r)} - 1 - \gamma(r) \tag{6}$$

where $\gamma(r) = h(r) - C(r)$. All repulsive core potentials are hard sphere, $U_{ij}(r) = \infty$ inside a distance of closest approach, and the exact constraint inside the hard core, $h_{ij}(r) = -1$ or $g_{ij}(r) = 0$, is enforced. Following prior PNC studies, we use the PY closure for all polymer−polymer and polymer−nanoparticle interactions (A−A, A−B, B−B, A−n, and B−n) and the HNC for filler−filler interactions.

Equation 4 in conjunction with the above closure relations defines a set of coupled nonlinear integral equations which are solved iteratively using an inexact Newton's method.[18,29] The polymer-mediated nanoparticle potential of mean force (PMF) then follows as

$$W_{nn}(r) = -\ln(g_{nn}(r)) \tag{7}$$

The second virial coefficient, normalized by its value for hard spheres in a vacuum, is

$$\overline{B}_2 = \frac{B_2}{B_{2,\text{HS}}} = \frac{-2\pi\int_0^\infty (g_{nn}(r) - 1)r^2\, dr}{4\pi D^3/6} = \frac{-3h_{nn}(k \rightarrow 0)}{4\pi D^3} \tag{8}$$

A lowest order virial analysis that neglects the small interfacial polymer−filler contributions (accurate for homopolymer nanocomposites[14,18]) yields a simple effective one-component particle description of spinodal phase separation at volume

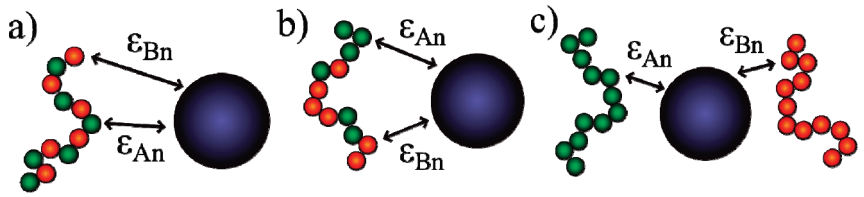

Figure 1. Conceptual cartoon of chemically heterogeneous systems, where the attraction strength between i and j sites is given by ε_{ij} and all unlabeled site−site interactions are hard core: (a) alternating AB copolymer, (b) random AB copolymer, and (c) A/B polymer blend.

fraction Φ_s

$$\Phi_s = -(8\overline{B_2}\eta_t)^{-1} \tag{9}$$

B. Intermolecular Site−Site Potentials. The chemistry of the system enters primarily via specification of the interparticle pair potentials. Here, all monomer−monomer interactions are taken to be hard core, and thus in absence of fillers all AB polymer models are equivalent to a homopolymer melt. This choice precludes polymer macrophase or microphase separation, allowing the effects of chemical attractions between each monomer type and the nanoparticle to be cleanly isolated. Particle−particle (diameter, D) interactions are also hard core, and the particle−polymer size asymmetry ratio is chosen to be $D/d = 5$ or 10. Thus, material chemistry enters only via the monomer−nanoparticle interactions, modeled as hard core with an exponential attraction:

$$U_{jn}(r) = \begin{cases} \infty, & r < r_c \\ -\varepsilon_{jn} e^{-(r-r_c)/\alpha_{jn}}, & r \geq r_c \end{cases} \tag{10}$$

where j = A or B and $r_c = (d + D)/2$ is the monomer−nanoparticle distance of closest approach (contact). The parameter ε_{jn} defines the contact adsorption strength, and α_{jn} is the spatial range of the interfacial attraction. The former describes the effective change in energy upon transferring a monomer from the bulk melt to the nanoparticle surface. The only difference between the A and B monomers is their attraction strength with the filler, ε_{An} or ε_{Bn}.

Experimentally realizable AB copolymers composed of chemically distinct A and B monomers will not have identical monomer−monomer interactions. In many cases, such as microphase-separating block copolymers, the net A−B repulsion is sufficiently large to qualitatively change the polymer morphology compared with the homogeneous A or B homopolymer melt. Moreover, even relatively small A−B repulsions could have important effects on nanoparticle effective interactions in blends and random copolymer melts. Here we are generally interested in systems where A and B monomers experience a difference in filler attraction strength that is much larger than the differences in monomer−monomer interactions, such as in refs 7−10 or a mixture with C_{60} nanoparticles, where the A and B copolymer monomers are chemically similar but experience very different attractions with the filler due to a specific interaction associated with a small part of the monomer. Working in the limit where all monomer−monomer interactions are exactly equal allows the effect of disparate filler−monomer interactions to be isolated and also affords a cleaner comparison between copolymers of varying sequences. It for these reasons we study the simple interaction model in this first study of nanoparticles in chemically heterogeneous, nonmicrophase-separating polymer melts. Nothing prevents PRISM theory from being employed in the future to account for system-specific differences in the intermonomer attractions.

A sketch of the systems studied is given in Figure 1. As motivation for the usefulness of using only a single chemical parameter for each monomer species, we note that PRISM theory predictions for the nanoparticle scattering structure factor of silica particles in poly(ethylene oxide) (PEO) and polytetrahydrofuran (PTHF) melts are in excellent agreement with experiment.[20] Decreasing ε_{pn} with all other PRISM parameters held constant was shown to reproduce the microstructural changes observed when changing from PEO to the more hydrophobic and weaker adsorbing PTHF matrix. The spatial range of both A and B monomer−filler interactions does impact polymer-mediated effects in a quantitative manner.[13−18] Here, we fix it at the (realistic) value used in recent work, $\alpha_{An} = \alpha_{Bn} = 0.5$. In the dilute nanoparticle limit it is trivial to include a more complex direct interfiller potential between a pair of spheres,[13] as relevant for specific quantitative applications to nanoparticles such as C_{60} or silica.

C. Chemically Heterogeneous Regimes. Prior PRISM theory work has established three primary forms of the polymer-mediated interaction and nanoparticle organization in a homopolymer melt: depletion and contact aggregation (d), steric stabilization via an adsorbed layer which induces a repulsive PMF (s), and tight polymer-mediated nanoparticle bridging (b), corresponding to small, intermediate, and large segment adsorption energy, respectively. We are interested in AB copolymers where the A and B monomer attraction strengths can be in different regimes corresponding to (d,s), (d,b), and (s,b). These three cases have built in (via the chain bonding constraints) energetic frustration with regards to polymer−particle interface wettability, the consequences of which will be copolymer sequence and composition dependent. How the system chooses the optimum (minimum free energy) spatial organization of copolymers around an isolated nanoparticle, and the corresponding polymer-mediated PMF, are the questions of prime interest.

As relevant background, Figure 2 shows the reference homopolymer-induced PMF for $D/d = 5$ at $\varepsilon_{pn} = 0$, 0.5, 1, 2, and 3, which vary in form from depletion to bridging. The inset shows selected polymer−particle site−site pair correlation functions. Analogous results at $D/d = 10$ are not shown since the latter are nearly the same (on the scale of the plot) at both values of D/d, and the PMF scales nearly linearly with D/d. Steric stabilization (repulsive PMF) behavior via equilibrium discrete adsorbed polymer layers occurs for $\varepsilon_{pn} = 0.5$. Here, $g_{pn} \sim 3$ at contact and quickly decays to the random value of unity, with small monomer scale oscillations, corresponding to moderate interfacial adsorption. Decreasing ε_{pn} to zero results in a reduced g_{pn} near contact and a contact depletion attraction in the PMF. A clear bridging regime is realized for $\varepsilon_{pn} = 3$, where g_{pn} at contact is

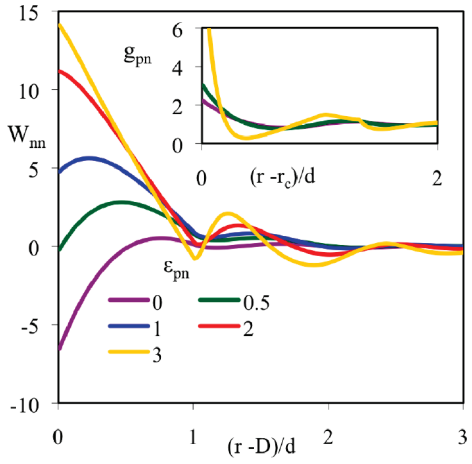

Figure 2. Particle−particle potential of mean force and monomer−particle correlation function (inset) as a function of the dimensionless surface-to-surface separation for dilute hard spheres of $D/d = 5$ in a homopolymer melt at the indicated values of ε_{pn}. The contact value of g_{pn} at $\varepsilon_{pn} = 3$ is ∼11.

significantly larger due to stronger adsorption, and the PMF is repulsive at short interparticle separations with oscillations and local attractive minima at longer distances corresponding to the sharing of adsorbed polymer between nanoparticles.

D. Polymer Matrices. To establish the role of copolymer sequence at fixed chemistry, calculations will be performed for four different polymer melt models: (i) pure A and B homopolymer, (ii) alternating AB copolymer (block length of unity), (iii) completely random AB copolymer, and (iv) A/B homopolymer blend. System ii is studied for the compositionally symmetric case ($f_A = 1/2$), and blend calculations are performed at 50/50 composition and equal A and B homopolymer chain lengths. In addition, for $f_A = 1/2$ we study a hypothetical "average homopolymer" defined as a chemically homogeneous chain that interacts with the nanoparticle via a mean attraction energy: $\bar{\varepsilon}_{pn} \equiv (\varepsilon_{An} + \varepsilon_{Bn})/2$. Understanding the behavior of this system provides insight as to whether the chemical heterogeneity is "statistically averaged" with regards to the packing of polymers around an isolated nanoparticle and the polymer-mediated PMF.

III. MONOMER−FILLER PACKING CORRELATIONS

A. Alternating Copolymers. On length scales larger than $2d$, we speculate that self-averaging effects may result in the $g_{in}(r)$ of alternating copolymers looking like the average homopolymer with a mean interfacial attraction energy of $\bar{\varepsilon}_{pn} = (\varepsilon_{An} + \varepsilon_{Bn})/2$. Figure 3 compares the two monomer−nanoparticle pair correlation functions, g_{An} and g_{Bn}, for an alternating copolymer with $\varepsilon_{Bn} = 0.5$, $\varepsilon_{An} = 0$ and 3 to the analogous average homopolymer result (g_{pn}, dashed lines) for (a) $D/d = 5$ and (b) $D/d = 10$. Note that intermediate between these results, at $\varepsilon_{An} = 0.5$, g_{An} and g_{Bn} are identical and equal to the homopolymer result at $\varepsilon_{pn} = 0.5$, shown in the inset to Figure 2. As expected, the polymer−particle correlation functions are similar for the two nanoparticle sizes. When $\varepsilon_{An} = 0$, the B monomers prefer the particle surface and the contact value of g_{An} is decreased, while that of g_{Bn} increased, relative to the homopolymer. These curves cross around a monomer−particle intersurface distance of one-half a monomer diameter, and the A monomer is very slightly more likely to be one monomer diameter from the particle than the B monomer. For $\varepsilon_{An} = 3$, the A monomers preferentially adsorb and g_{An} and g_{Bn} curves again cross at a distance equal to a fraction of a monomer diameter and cross again for separation between 1 and $2d$, before becoming approximately equal for $r > 2d$. This curve crossing is caused by the alternating nature of the copolymer, i.e., whereas A monomers are highly likely to be at the particle surface, the B monomers to which they are directly connected are more likely to be a short distance from the surface. In either case, we find the average of g_{An} and g_{Bn} (not shown) is very similar to g_{pn} of the averaged homopolymer, further supporting the self-averaging idea.

B. Random Copolymers. Figure 4 shows both monomer−particle pair correlation functions for a random AB copolymer of symmetric composition ($f_A = 0.5$) with $\varepsilon_{Bn} = 0.5$ and variable ε_{An} for $D/d = 5$. We again find that particle diameter has little effect, and hence the analogous $D/d = 10$ correlation functions are not shown. Relative to the average homopolymer, g_{An} is reduced at contact to ∼2 and g_{Bn} is increased; however, the shape of both correlation functions remains similar and almost equivalent at distances greater than one monomer diameter from the surface. The average of g_{An} and g_{Bn} (not shown) for this $\varepsilon_{An} = 0$ and $\varepsilon_{Bn} = 0.5$ case is approximately equal to the homopolymer g_{pn} at the mean $\varepsilon_{pn} = 0.25$. Increasing ε_{An} to 3 dramatically increases g_{An} at contact and reduces g_{Bn}; g_{An} now remains larger than g_{Bn} out to almost 2 monomer diameters, and averaging the two correlation functions yields an increased contact value and other small differences compared with the preaveraged $\varepsilon_{pn} = 1.75$ effective homopolymer result.

The above trends reflect physics unique to sequence disordered random copolymers. Specifically, in random AB copolymers there must statistically exist some locally blocky structures composed of runs of several A (or B) connected monomers. Such configurations allow for a continuous excess of g_{An} over g_{Bn}, or the averaged homopolymer g_{pn}, out to a length scale of order several monomer diameters. Local stretches of A monomers can preferentially adsorb on the nanoparticles, and hence a much greater local f_A can be realized near the filler surface than in the bulk. This effect cannot occur for alternating copolymers on length scales larger than d. Therefore, the effective interaction of a nanoparticle with the surrounding polymer will be closer to that of a homopolymer of the more strongly adsorbing monomer for random copolymers, in contrast to the simpler alternating copolymer behavior. This physical picture is also consistent with our finding that the average of the alternating copolymer g_{An} and g_{Bn} is more similar to the averaged homopolymer result than is the average of these quantities for the random copolymer.

C. Binary Blend. Obviously, a polymer blend contains much longer continuous stretches of A or B monomers (the entire chain) than the random copolymer. Hence, A and B monomers can much more completely separate near the nanoparticle surface driven by preferential adsorption. Figure 5 presents calculations of the monomer−particle pair correlation functions. One sees g_{An} and g_{Bn} remain distinct for the blend over a much longer length scale than for the random copolymer. The blue lines are analogous to those of Figures 3 and 4 ($\varepsilon_{Bn} = 0.5$, $\varepsilon_{An} = 0$) and show an increased g_{Bn} and decreased g_{An} relative to these other cases, which persists out to $r \sim 8d$, well beyond the range of typical dense fluid monomer scale oscillations. In essence, "surface segregation" occurs. When ε_{An} is increased to 0.75, g_{Bn} is reduced so much that it becomes (unphysically) negative at a short distance, and hence we do not perform calculations beyond this attraction strength.

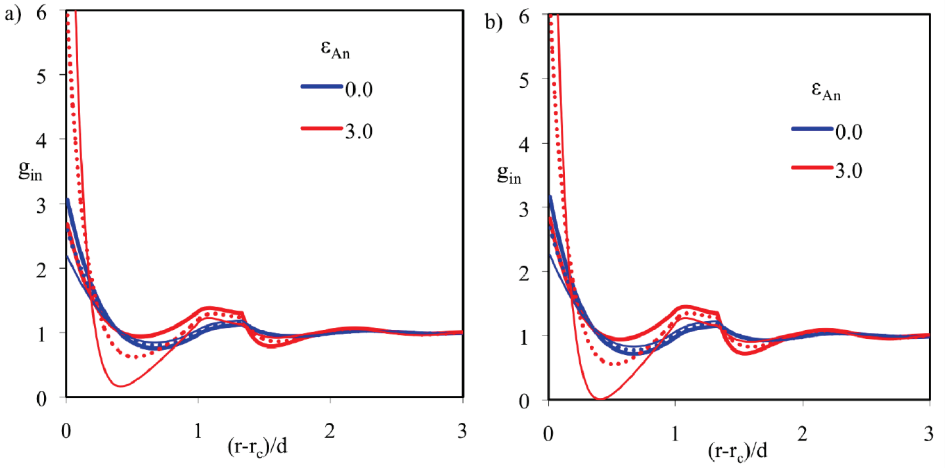

Figure 3. A (thin solid lines) and B (thick solid lines) monomer−particle correlation functions for dilute hard spheres of (a) $D/d = 5$ and (b) $D/d = 10$ in an alternating AB copolymer melt, with $f_A = 0.5$ and $\varepsilon_{Bn} = 0.5$ at the indicated values of ε_{An}, compared with the average homopolymer result (dotted lines, $\varepsilon_{Pn} = (\varepsilon_{An} + \varepsilon_{Bn})/2$). The contact value of g_{An} at $\varepsilon_{An} = 3$ is ∼12 for both (a) and (b).

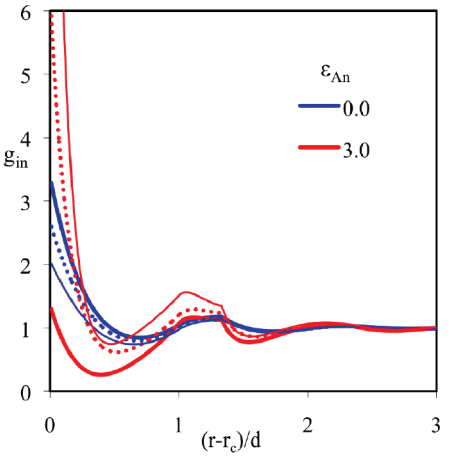

Figure 4. A (thin solid lines) and B (thick solid lines) monomer−particle correlation functions as a function of the dimensionless surface-to-surface separation of a monomer and nanoparticle for dilute hard spheres of $D/d = 5$ in a random AB copolymer, with $f_A = 0.5$ and $\varepsilon_{Bn} = 0.5$ at the indicated values of ε_{An}, compared with the average homopolymer result (dotted lines, $\varepsilon_{Pn} = (\varepsilon_{An} + \varepsilon_{Bn})/2$)). The contact value of g_{An} at $\varepsilon_{An} = 3$ is ∼16.

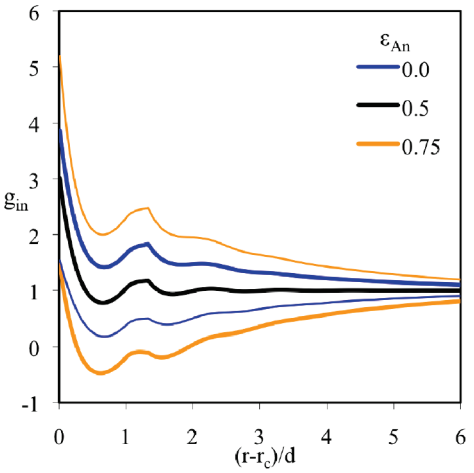

Figure 5. A (thin lines) and B (thick lines) monomer−particle correlation functions for dilute hard spheres of $D/d = 5$ in a blend with equal amounts of A and B polymer and $\varepsilon_{Bn} = 0.5$ at the indicated values of ε_{An}.

We note in passing that on a qualitative physical basis we expect the preferential adsorption effect promotes demixing in a binary polymer blend that can undergo macrophase separation in the absence of the nanoparticles. However, we cannot make any definitive statements since our calculations are performed under nanoparticle infinite dilution conditions.

IV. NANOPARTICLE POTENTIAL OF MEAN FORCE

We now compute the polymer-mediated PMF between nanoparticles for the systems studied in section III and additional cases. The effect of copolymer sequence is first examined under fixed symmetric composition conditions.

A. Effect of Copolymer Sequence for Symmetric Composition. Figure 6 shows the PMF for $D/d = 5$ induced by the alternating copolymer (solid lines) and the analogous average homopolymer (dotted lines) when $\varepsilon_{Bn} = 0.5$ and ε_{An} varies from 0 to 3. The alternating copolymer and average homopolymer results are similar, showing the typical depletion, steric stabilization, and weak bridging behavior as ε_{An} increases. At higher ε_{An} values there are quantitative differences: the alternating copolymer PMF has a smaller contact repulsion, an enhanced repulsion for separations between 1 and $2d$, and a reduced bridging strength. These differences are due to the tighter adsorption of A and weaker layering of B monomers around the nanoparticle surface; the steric constraint of a less adsorbing B monomer attached to every A frustrates the preferential packing of A on the surfaces of two nanoparticles close in space.

The random (solid curves) and alternating (dotted curves) copolymer-induced PMF results are compared in Figure 7 for $f_A = 0.5$, $\varepsilon_{Bn} = 0.5$, and ε_{An} varying from 0 to 3. At $\varepsilon_{An} = 0$, the alternating and random copolymer results are similar. For the alternating copolymer, increasing ε_{An} monotonically increases

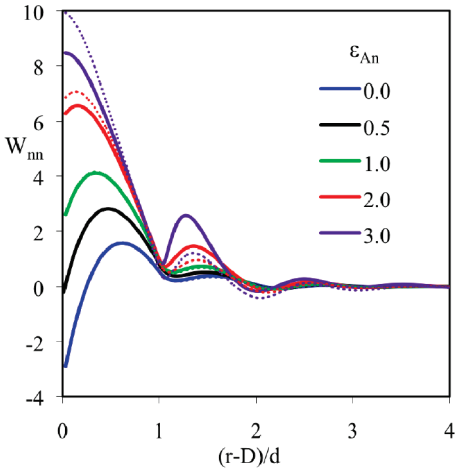

Figure 6. Potential of mean force for dilute hard spheres of $D/d = 5$ in an alternating AB copolymer melt (solid lines), with $f_A = 0.5$ and $\varepsilon_{Bn} = 0.5$ at the indicated values of ε_{An}, compared with the average homopolymer result (dotted lines, $\varepsilon_{Pn} = (\varepsilon_{An} + \varepsilon_{Bn})/2)$) which lies on top of the alternating copolymer PMF on the scale of this figure for $\varepsilon_{An} = 0-1$.

the PMF at short interparticle distances, though at large $\varepsilon_{An} = 2$ and 3 a very small bridging minimum develops at $\sim 2d$. For the random copolymer, increasing ε_{An} initially enhances the near contact region of the PMF in a similar manner, but at $\varepsilon_{An} = 2$ and 3 the behavior becomes starkly different. Specifically, the contact value of the PMF decreases, and a deep, relatively long-range ($\sim 3d$) bridging minimum emerges. Although there are small monomer scale oscillations overlaid on the PMF, it remains negative (attractive) out to several monomer diameter separations. This corresponds to a qualitatively different type of behavior than the multiple bridging minima with monomer scale oscillations that occur symmetrically (oscillate about zero) for highly attractive homopolymers.[13] Apparently, as the nanoparticles approach in a random copolymer melt, local runs of A monomers in the copolymer chain can form a strongly adsorbing bridge extending over several monomer diameters. This behavior is not possible for either the alternating copolymer or homopolymer matrix until ε_{pn} is very large (larger than the average of ε_{An} and ε_{Bn} of a strongly bridged random polymer). A conceptual sketch of such a bridging configuration in the alternating copolymer, random copolymer, and polymer blend is presented in Figure 8. We find this strong bridging form of the PMF also approximately scales linearly with D/d, a fact that could have important kinetic consequences, e.g., the emergence of a kinetic barrier to weak bridging which is significantly higher for bigger nanoparticles.

Another notable feature of Figure 7 is the rather dramatic change in the form of the PMF over the relatively narrow range of $\varepsilon_{An} = 1-2$. Detailed calculations (not shown) reveal this change in behavior does not occur in any "critical" or discontinuous manner, but rather as a smooth function of the attraction strength between the A monomer and nanoparticle. Moreover, this change of PMF behavior is very similar for the $D/d = 5$ and 10 systems, emphasizing its fundamentally local nature.

As expected from the calculations in section IIIC, Figure 9 shows a much longer range PMF for polymer blends. The $\varepsilon_{An} = 0$ and $\varepsilon_{Bn} = 0.5$ system has a depletion minimum similar to that of the random, alternating, and averaged homopolymer cases. However, beyond the small separation where the weak repulsion peak occurs, a broad bridging minimum emerges, in qualitative contrast to all prior results. It seems that although the adsorption strength is not large and depletion attraction remains, since the A and B monomers are not connected the more adsorbing species strongly accumulates near the particles and prefers to bridge the fillers, a state of organization which allows the less adsorbing polymer to increase its entropy. For $\varepsilon_{An} = 0.75$ and $\varepsilon_{Bn} = 0.5$, a much deeper bridging minimum is observed. The PMF again nearly scales linearly with D/d.

B. Effect of Copolymer Composition. Figures 10−12 explore the effect of random copolymer composition on the PMF for $D/d = 5$; Figure 11b shows the corresponding results for $D/d = 10$. In each figure, ε_{An} and ε_{Bn} are chosen to place the A and B monomers in different regimes of corresponding homopolymer behavior: depletion/stabilization (Figure 10), bridging/stabilization (Figure 11), and bridging/depletion (Figure 12). In all cases the PMF approximately scales linearly with D/d.

Figure 10 shows the depletion/stabilization case of $\varepsilon_{An} = 0$ and $\varepsilon_{Bn} = 0.5$ with random copolymer composition varying from $f_A = 0.01$ (nearly steric stabilizing homopolymer limit) to $f_A = 0.99$ (nearly nonadsorbing homopolymer limit). These extreme composition PMF curves are very similar to the analogous homopolymer results in Figure 2. The PMF undergoes a smooth transition from pure steric stabilization to pure depletion with increasing A monomer concentration. Interestingly, even at intermediate values of f_A where frustration is largest, the PMF is reasonably well predicted by a simple interpolation of the $f_A = 0.01$ and 0.99 curves.

The analogous results for the bridging/stabilization copolymer system with $\varepsilon_{An} = 3$ and $\varepsilon_{Bn} = 0.5$ are shown in Figure 11. The PMFs display qualitatively different and noninterpolative behavior compared to the depletion/stabilization system. At $f_A = 0.01$, it is very similar to that of the $\varepsilon_{pn} = 3$ homopolymer (Figure 2). However, the PMF of the $f_A = 0.99$ system is decreased somewhat relative to the $\varepsilon_{pn} = 0.5$ homopolymer result for filler surface-to-surface separations of 1−2 monomer diameters. This additional attraction may be caused by the sharing of single attractive B monomers between nanoparticles or statistically rare B-rich chain sequences in the random copolymer. The PMF results for intermediate $f_A = 0.25-0.75$ are starkly different than a simple interpolation between the $f_A = 0.01$ and 0.99 limits would predict. Instead, the curves have a similar shape to the PMF of the $f_A = 0.01$system but are greatly decreased (more attractive) out to filler surface-to-surface separations of $\sim 2.5d$, an effect first seen in Figure 7. The new strong bridging minimum monotonically deepens as the fraction of strongly attractive monomers (f_A) is reduced from 0.75 to 0.25. Even at relatively low $f_A = 0.25$, stretches of several A monomers are present in the random copolymer, which again drive this novel long-range bridging behavior; for this case, the adsorbing patches are preferentially pushed to the particle surface by the less adsorbing monomer for entropic reasons, thereby resulting in an even stronger bridging state than in the corresponding pure homopolymer.

Figure 12 presents the PMF results for the bridging/depletion copolymer, $\varepsilon_{An} = 3$ and $\varepsilon_{Bn} = 0$. As in Figure 11, the $f_A = 0.01$ curve is decreased at short distances relative to the $f_A = 0$ homopolymer. Also similar to Figure 11, decreasing f_A from 0.99 to 0.25 results in a monotonically stronger attraction in the PMF which is largest at contact and persists out to $\sim 2.5d$. The difference between the A and B monomers is now greater than in

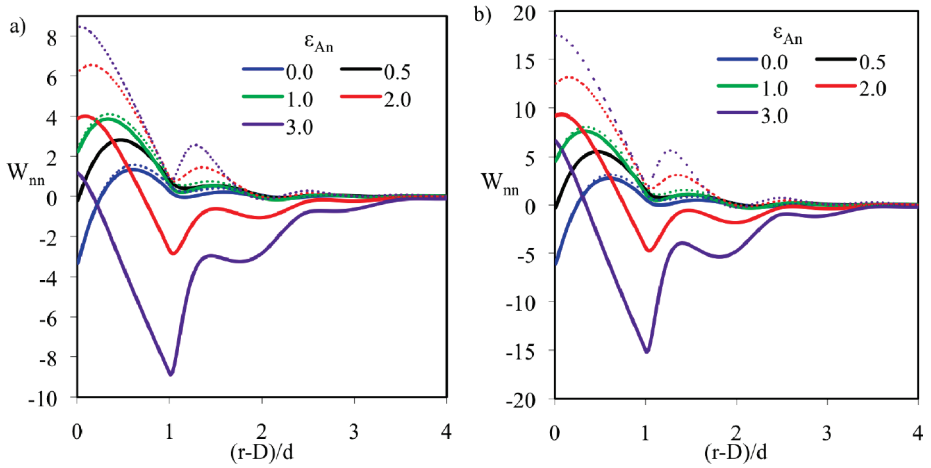

Figure 7. Potential of mean force for dilute hard spheres of (a) $D/d = 5$ and (b) $D/d = 10$ in a random (solid lines) or alternating (dotted lines) AB copolymer melt, with $f_A = 0.5$ and $\varepsilon_{Bn} = 0.5$ at the indicated values of ε_{An}.

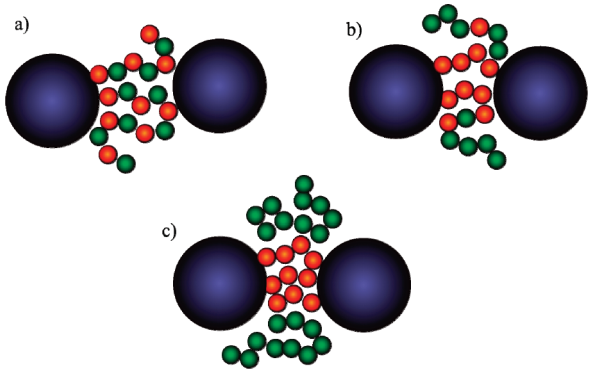

Figure 8. Sketches of possible polymer bridging configurations between two nanoparticles for (a) alternating copolymer, (b) random copolymer, and (c) polymer blend.

the bridging/stabilization case, and the novel bridging behavior is even more dramatic.

V. MISCIBILITY

We now analyze spinodal phase separation in the dilute virial framework discussed in section IIA. The key quantity is the normalized nanoparticle second virial coefficient. Results are shown in Figure 13 for random and alternating copolymers of $f_A = 0.5$ as a function of increasing ε_{An} at a fixed $\varepsilon_{Bn} = 0$; the averaged homopolymer analogue is also plotted. At low ε_{An}, depletion attraction reduces miscibility and $\overline{B_2}$ is small (negative). Increasing ε_{An} leads to $\overline{B_2} > 1$, indicating that a discrete adsorbed polymer layer forms which induces a repulsive PMF, increases the effective nanoparticle diameter, and ensures complete miscibility. At high ε_{pn}, $\overline{B_2}$ decreases, now due to a bridging attraction between particles. $\overline{B_2}$ eventually becomes negative beyond $\varepsilon_{pn} \sim 3-4$ for the homopolymer at both values of D/d. For alternating copolymers, the trends are similar, but $\overline{B_2}$ is even greater than the homopolymer result until it decreases sharply after $\varepsilon_{An} = 6$. However, as is evident from the strong bridging features in the PMF, $\overline{B_2}$ of random copolymers decreases suddenly at moderate ε_{An} and is large and negative at $\varepsilon_{An} = 2$.

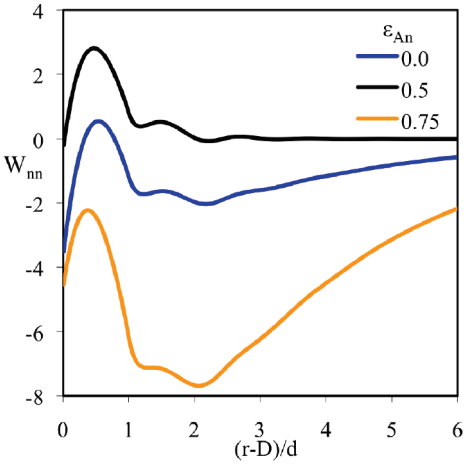

Figure 9. Potential of mean force for dilute hard spheres of $D/d = 5$ in a blend of equal amounts of A and B homopolymer with $\varepsilon_{Bn} = 0.5$ at the indicated values of ε_{An}.

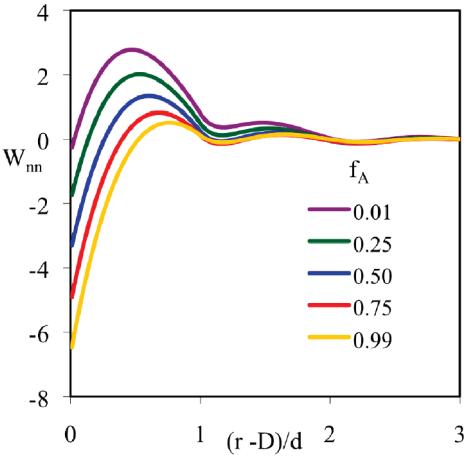

Figure 10. Potential of mean force for dilute hard spheres of $D/d = 5$ in a random AB copolymer melt with various f_A at $\varepsilon_{An} = 0$ and $\varepsilon_{Bn} = 0.5$.

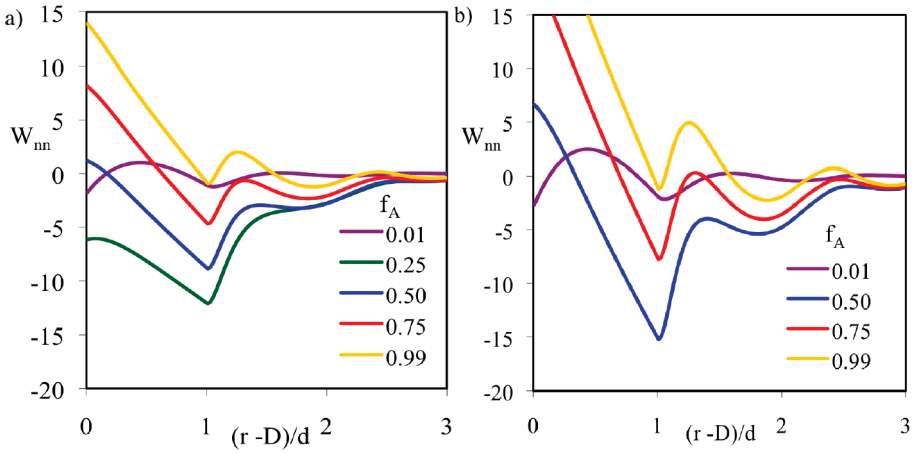

Figure 11. Potential of mean force for dilute hard spheres of (a) $D/d = 5$ and (b) $D/d = 10$, in a random AB copolymer melt at with various f_A with $\varepsilon_{An} = 3$ and $\varepsilon_{Bn} = 0.5$. The $D/d = 10$, $f_A = 0.25$ system could not be numerically converged.

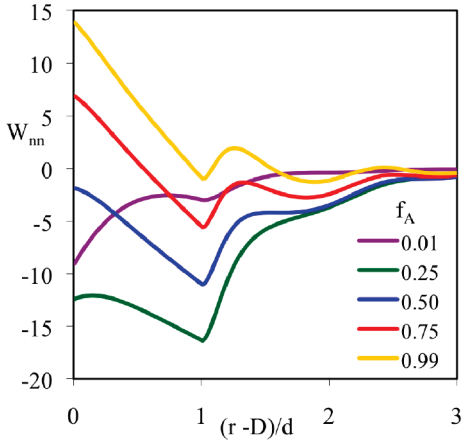

Figure 12. Potential of mean force for dilute hard spheres of $D/d = 5$ in a random AB copolymer melt, at various f_A with $\varepsilon_{An} = 3$ and $\varepsilon_{Bn} = 0$.

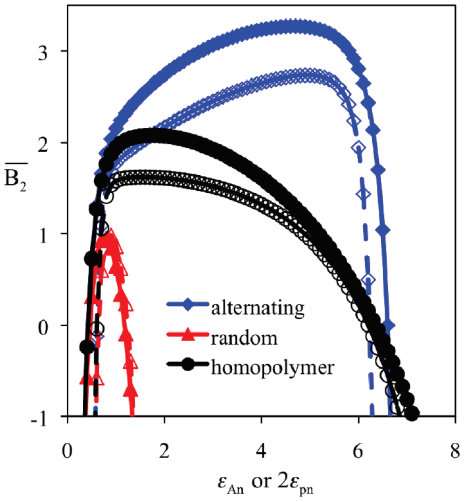

Figure 13. Normalized second virial coefficient for random and alternating copolymer melts at $f_A = 0.5$ and $\varepsilon_{Bn} = 0$ as a function ofε_{An}; solid lines are at $D/d = 5$, and dashed are for $D/d = 10$. Black lines compare to the averaged ($\varepsilon_{pn} = \varepsilon_{An}/2$) homopolymer case.

The normalized second virial coefficients and the associated virial predictions of the spinodal phase separation nanoparticle volume fractions (eq 9) are reported in Table 1 for the random copolymer, alternating copolymer, and reference homopolymer. The bridging/depletion and bridging/stabilization random copolymer cases show a large negative $\overline{B_2}$ at intermediate f_A corresponding to the novel deep bridging minimum PMF behavior and hence almost complete immiscibility. On the other hand, the depletion/stabilization random copolymer case shows monotonically increasing miscibility as the fraction of adsorbing monomer grows.

It is interesting to compare the behavior of the alternating copolymer to the corresponding pure homopolymers. In Figure 13, the B homopolymer corresponds to $\varepsilon_{Bn} = 0$, which induces a strong depletion attraction and a large negative $\overline{B_2}$ (Table 1). When $\varepsilon_{An} > 3.2$, the A homopolymer also yields a negative $\overline{B_2}$. However, construction of an alternating copolymer using these two monomers results in a positive $\overline{B_2}$ up to $\varepsilon_{An} = 6.6$ (6.2 for $D/d = 10$), an enormously nonadditive effect! The strong A−filler attraction apparently increases polymer adsorption, while the A−B layering effect around particles prevents bridging that would be present for the pure A homopolymer system. The large $\overline{B_2}$ suggests an adsorbed polymer layer thicker than what occurs for the averaged homopolymer over most of the miscibility window.

In contrast to the above behavior, we do not find any set of parameters where nanoparticles are the most miscible for an intermediate composition of a AB random copolymer compared to the reference A or B homopolymers. This differs from the recent experimental observation of increased miscibility of functionalized carbon nanotubes dissolved in random copolymers containing a monomer with a specific interaction with CNTs. Besides the obvious differences compared with our study associated with the rodlike nature of CNTs and the likely presence of nonequilibrium kinetic effects, the major distinction is that the specific filler−copolymer interaction is not the only difference between the monomers of the copolymer. The change in intermolecular interactions of the copolymer with composition are thought to be relevant.[8] Furthermore, in the experimental systems, very local steric constraints affect how nearby monomers can interact with the filler in a manner that likely cannot be captured by a simple freely jointed chain model.[9] The

dx.doi.org/10.1021/ma200079z |*Macromolecules* 2011, 44, 3149–3160

Table 1. Normalized Second Virial Coefficient and Spinodal Nanoparticle Volume Fraction for Two Values of the Size Asymmetry Ratio, D/d, and Various Copolymer Compositions and Monomer−Nanoparticle Attraction Strengths[a]

				$D/d = 5$		$D/d = 10$	
architecture	f_A	ε_{An}	ε_{Bn}	$B_2/B_{2,HS}$	Φ_s	$B_2/B_{2,HS}$	Φ_s
homopolymer	1	0	0	−24.4	0.01	-2.4×10^3	1.3×10^{-4}
homopolymer	1	0.25	0.25	0.73	miscible	−3.53	0.09
homopolymer	1	0.5	0.5	1.95	miscible	1.58	miscible
homopolymer	1	0.75	0.75	2.07	miscible	1.62	miscible
homopolymer	1	1.25	1.25	2.02	miscible	1.58	miscible
homopolymer	1	1.75	1.75	1.79	miscible	1.44	miscible
homopolymer	1	3	3	0.35	miscible	0.22	miscible
alternating	0.5	0	0.5	0.73	miscible	−3.83	0.08
alternating	0.5	1	0.5	2.13	miscible	1.67	miscible
alternating	0.5	2	0.5	2.39	miscible	1.88	miscible
alternating	0.5	3	0.5	2.57	miscible	2.08	miscible
random	0.5	0	0.5	0.31	miscible	−4.30	0.07
random	0.5	1	0.5	1.84	miscible	1.51	miscible
random	0.5	2	0.5	−3.98	0.08	−6.78	0.05
random	0.5	3	0.5	-1.0×10^3	3.1×10^{-4}	-1.3×10^5	2.5×10^{-6}
blend	0.5	0.75	0.5	-3.8×10^3	8.3×10^{-5}	-1.8×10^5	1.7×10^{-6}
blend	0.5	0	0.5	−31.06	0.01	−34.71	9.0×10^{-3}
random	0.01	0	0.5	1.93	miscible	1.57	miscible
random	0.25	0	0.5	1.49	miscible	1.18	miscible
random	0.5	0	0.5	0.31	miscible	−4.30	0.07
random	0.75	0	0.5	−4.22	0.07	-1.1×10^2	2.8×10^{-3}
random	0.99	0	0.5	−22.92	0.01		
random	0.01	3	0	-3.3×10^2	9.4×10^{-4}	-1.1×10^5	2.8×10^{-6}
random	0.25	3	0	-2.3×10^6	1.4×10^{-7}		
random	0.5	3	0	-8.7×10^3	3.6×10^{-5}		
random	0.75	3	0	−43.13	7.2×10^{-3}	-3.2×10^2	9.7×10^{-4}
random	0.99	3	0	0.12	miscible	0.02	miscible
random	0.01	3	0.5	0.24	miscible	0.34	miscible
random	0.25	3	0.5	-3.0×10^4	1.1×10^{-5}		
random	0.5	3	0.5	-1.0×10^3	3.1×10^{-4}	-1.3×10^5	2.5×10^{-6}
random	0.75	3	0.5	−19.34	0.02	−79.77	3.9×10^{-3}
random	0.99	3	0.5	0.17	miscible	0.07	miscible

[a] Gaps in the data at $D/d = 10$ are where numerical convergence of the integral equations could not be achieved.

electron donor−acceptor experimental system that produces the best CNT dispersion is a cyanostyrene−styrene copolymer of 24% cyanostyrene (cyanostyrene interacts strongly as an electron acceptor with CNTs, styrene does not). In our work, each monomer along the chain is available to adsorb on the filler(s) (although connectivity constraints and polymer entropy prevent an entire polymer chain from very closely adsorbing on a filler surface). The possibility of several A monomers occurring in a row in a random copolymer and simultaneously adsorbing to two fillers appears to drive the novel long-range bridging attraction discovered in section IV. However, for the cyanostyrene system this may not be possible. DFT calculations of a cyanostyrene trimer near a nanotube showed the middle monomer does not bind to the CNT due to steric constraints.[9] While it is not clear whether the middle monomer would be available to bind to another nanotube, these calculations suggest that A−A−A sequence steric considerations (at least) are relevant for the experimental system. One may speculate that if such considerations interfere with the novel long-range bridging effect deduced based on freely jointed chain random copolymers, the experimental system may behave more similarly to our alternating copolymers, in the sense that the composition predominantly acts to tune the overall polymer−filler interaction. In this case, we did observe increased miscibility for intermediate copolymer compositions compared with either homopolymer alone.

VI. SUMMARY AND CONCLUSIONS

The addition of chemical heterogeneity and/or sequence disorder to matrix polymers can qualitatively change effective interactions between nanoparticles and their degree of spatial dispersion. The comparison of various heterogeneous polymers, in which one type of monomer is more strongly adsorbing than the other, shows that these systems can induce dramatically different nanoparticle PMFs compared with the behavior of homopolymers. An alternating copolymer shows a small layering effect; i.e., the more strongly adsorbing monomer is likely to be closer the particle surface, while the other monomers are more

likely to be a short distance away. Chain connectivity plus differential wetting results in a small excess repulsion compared to the corresponding homogeneous "average homopolymer" characterized by an single mean interfacial attraction energy. However, the overall depletion−stabilization−bridging progression seen in homopolymers as interfacial attraction ε_{pn} is increased is qualitatively similar for alternating copolymers as adsorption strength is increased for one its monomers.

In contrast to alternating AB copolymers, both random copolymers and A/B blends can mediate a novel strong and long-range bridging behavior in the PMF which has no analogue in the pure homopolymer reference systems. The deep bridging minimum may start at contact (for low f_A of a random copolymer) or around one monomer diameter surface-to-surface separation, and persists out to $\sim 3d$ for random copolymers, and is even longer range ($\sim 6d$) for the polymer blend. For random copolymers this longer length scale is apparently due to runs of several adsorbing monomers that are statistically present in the copolymer conformation at intermediate f_A, an effect amplified in the blend where it is akin to local surface segregation or preferential wetting. The random copolymer and polymer blend calculations reveal that a very large monomer adsorption energy is not needed to induce a strong bridging minimum, and (surprisingly) bridging is stronger at an adsorbing monomer fraction of 0.25 than at 0.5 for the random copolymer. Obviously, the alternating copolymer does not have long stretches of the same adsorbing monomer, and hence in these systems the strong and long-range bridging attraction is not observed, and an "average homopolymer" description is a reasonably accurate zeroth-order approximation.

Our results collectively indicate that the nonadsorbing, or less strongly adsorbing, monomers are crucial to the predicted new copolymer bridging behavior. The more adsorbing polymers are driven to the filler surface by both energetic considerations and the entropic gain of the less adsorbing monomers which are not as close to the impenetrable particle surface. This results in an effectively thicker adsorbed polymer layer than for homopolymers and a very strong bridging attraction when this layer is shared between nanoparticles. Both copolymer composition and sequence play crucial roles in determining the polymer-induced PMF between nanoparticles, and therefore the details of copolymer architecture should be a key consideration in the design of nanocomposites based on chemically heterogeneous polymers.

The present work represents our initial effort to understand how the chemical heterogeneity of matrix copolymers that do not microphase separate influences effective nanoparticle interactions. We have studied a very simple model, and of course there are many open questions and avenues for future work. In the dilute nanoparticle limit, the most immediate is to study the consequences of changing the interfacial attraction range and adding in direct internanoparticle interactions (generally attractive van der Waals for bare particles). These features are highly material specific and, for example, are very different for small nanoparticles such as C_{60} (where D/d is only ~ 2) versus larger nanoparticles such as silica (where typically $D/d \sim 10-100$). Another interesting issue is the role of block length in regular multiblock AB copolymers. Preliminary calculations[30] find a strong coupling of block size, nanoparticle size, and the interfacial monomer−particle attractions with regards to the form of the PMF; distinct behavior occurs depending on whether the block length is smaller or larger than the nanoparticle. In addition, there will be many experimentally relevant cases where a net repulsion (positive Flory chi-parameter) of variable magnitude exists between the A and B monomers, the conseqeunces of which will be coupled with monomer−nanoparticle differential wettability to determine the PMF. This aspect is also of interest to study under dilute nanoparticle conditions. Ultimately, for those systems identified as miscible in the present or future work, a full PRISM theory study of pair correlations and scattering structure factors at nonzero filler volume fractions will be interesting to perform. In particular, the new questions of how interpolymer correlations (AA, AB, BB) change as a function of nanoparticle volume fraction, and whether many-body effects can lead to phase separation at elevated filler loadings, naturally arise. Moreover, if the matrix copolymers themselves can microphase (or macrophase) separate, then whether nanoparticle addition enhances or suppresses this phenomenon is of interest. Finally, building on our prior work,[16] how copolymers of various sequence and composition mediate interactions between nonspherical particles of various shapes is of high interest.

AUTHOR INFORMATION

Corresponding Author

*E-mail: kschweiz@illinois.edu.

Present Addresses

§Sandia National Laboratories, Albuquerque, NM 87185.

ACKNOWLEDGMENT

We thank Mark Dadmun and Bobby Sumpter for motivating discussions and explanations of their recent experimental and computational results. We also thank Debapriya Banerjee for several insightful discussions and comments. This work was funded by the Materials Science and Engineering division of DOE-BES via Oak Ridge National Laboratory.

REFERENCES

(1) Winey, K. I.; Vaia, R. A. *MRS Bull.* **2007**, *32*, 314–319.

(2) Mackay, M. E.; Tuteja, A.; Duxbury, P. M.; Hawker, C. J.; Horn, B. V.; Guan, Z.; Chen, G.; Krishnan, R. S. *Science* **2006**, *311*, 1740–1743.

(3) Balazs, A. C.; Emrick, T.; Russell, T. P. *Science* **2006**, *314*, 1107–1110.

(4) Haryono, A.; Binder, W. H. *Small* **2006**, *2*, 600–611. Sknepnek, R.; Anderson, J. A.; Lamm, M. H.; Schmalian, J.; Travesset, A. *ACS Nano* **2008**, 1259–1265.

(5) Listak, J.; Hakem, I. F.; Ryu, H. J.; Rangou, S.; Politakos, N.; Misichronis, K.; Avgeropoulos, A.; Bockstaller, M. R. *Macromolecules* **2009**, *42*, 5766–5773.

(6) Zhang, L.; Lin, J. *Macromolecules* **2009**, *42*, 1410–1414.

(7) Eastwood, E.; Viswanathan, S.; O'Brien, C. P.; Kumar, D.; Dadmun, M. D. *Polymer* **2005**, *46*, 3957–3970.

(8) Rasheed, A.; Chae, H. G.; Kumar, S.; Dadmun, M. D. *Polymer* **2006**, *47*, 4734–4741.

(9) Linton, D.; Driva, P.; Sumpter, B.; Ivanov, I.; Geohegan, D.; Feigerle, C.; Dadmun, M. D. *Soft Matter* **2010**, *6*, 2801–2814.

(10) Rasheed, A.; Dadmun, M. D.; Ivanov, I.; Britt, P. F.; Geohegan, D. B. *Chem. Mater.* **2006**, *18*, 3513–3522.

(11) Schweizer, K. S.; Curro, J. G. *Adv. Chem. Phys.* **1997**, *98*, 1–142.

(12) Hooper, J. B.; Schweizer, K. S.; Desai, T. G.; Koshy, R.; Keblinski, P. *J. Chem. Phys.* **2004**, *121*, 6986–6997.

(13) Hooper, J. B.; Schweizer, K. S. *Macromolecules* **2005**, *38*, 8858–8869.

(14) Hooper, J. B.; Schweizer, K. S. *Macromolecules* **2006**, *39*, 5133–5142.

(15) Hooper, J. B.; Schweizer, K. S. *Macromolecules* **2007**, *40*, 6998–7008.
(16) Hall, L. M.; Schweizer, K. S. *Soft Matter* **2010**, *6*, 1015–1025.
(17) Zhao, L.; Li, Y.-G.; Zhong, C.; Mi, J. *J. Chem. Phys.* **2006**, *124*, 144913.
(18) Hall, L. M.; Schweizer, K. S. *J. Chem. Phys.* **2008**, *128*, 234901.
(19) Sen, S.; Xie, Y.; Kumar, S. K.; Yang, H.; Bansal, A.; Ho, D. L.; Hall, L.; Hooper, J. B.; Schweizer, K. S. *Phys. Rev. Lett.* **2007**, *98*, 128302.
(20) Hall, L. M.; Anderson, B. J.; Zukoski, C. F.; Schweizer, K. S. *Macromolecules* **2009**, *42*, 8435–8442.
(21) Kim, S. Y.; Hall, L. M.; Schweizer, K. S.; Zukoski, C. F. *Macromolecules* **2010**, *43*, 10123–10131.
(22) Ganesan, V.; Ellison, C. J.; Pryamitsyn, V. *Soft Matter* **2010**, *6*, 4010–4025.
(23) Hall, L. M.; Jayaraman, A.; Schweizer, K. S. *Curr. Opin. Solid State Mater. Sci.* **2010**, *14*, 38–48.
(24) Schweizer, K. S.; Yethiraj, A. *J. Chem. Phys.* **1993**, *98*, 9053–9079.
(25) (a) David, E. F.; Schweizer, K. S. *Macromolecules* **1997**, *30*, 5118–5132. (b) Guenza, M.; Schweizer, K. S. *Macromolecules* **1997**, *30*, 4205–4219.
(26) Kolbet, K. A.; Schweizer, K. S. *Macromolecules* **2000**, *33*, 1425–1442; 1443–1458.
(27) Sung, B. J.; Yethiraj, A. *Macromolecules* **2005**, *38*, 2000–2008.
(28) Chandler, D.; Andersen, H. C. *J. Chem. Phys.* **1972**, *57*, 1930–1937.
(29) Hall, L. M. Ph.D.Thesis, University of Illinois at Urbana—Champaign, 2009.
(30) Banerjee, D.; Hall, L. M.; Schweizer, K. S., unpublished.